



**Controlled Synthesis of Mesoporous Nitrogen-Doped
Carbons with Highly Ordered Two-Dimensional Hexagonal
Mesostructures and Their Chemical Activation**

Journal:	<i>Nanoscale</i>
Manuscript ID	NR-ART-04-2018-002647.R1
Article Type:	Paper
Date Submitted by the Author:	22-May-2018
Complete List of Authors:	<p>Allah, Abeer; National Institute for Materials Science, WPI Center for MANA Tan, Haibo; National Institute for Materials Science, WPI Center for MANA Xu, Xingtao; National Institute for Materials Science, WPI Center for MANA Farghali, Ahmed; Beni Suef University Khedr, Mohamed; Dean of faculty of postgraduate studies for advanced sciences Alshehri, Abdulmohsen; King Abdulaziz University, Chemistry Bando, Yoshio; National Inst for Materials Science, Advanced Materials Lab and Nanomat Lab Nanjundan, Ashok Kumar; University of Queensland, Australian Institute for Bioengineering & Nanotechnology; University of Queensland, School of Chemical Engineering Yamauchi, Yusuke; University of Queensland Australian Institute for Bioengineering and Nanotechnology, ; National Institute for Materials Science, WPI Center for MANA</p>

Controlled Synthesis of Mesoporous Nitrogen-Doped Carbons with Highly Ordered Two-Dimensional Hexagonal Mesostructures and Their Chemical Activation

Abeer Enaiet Allah,^{†1,2} Haibo Tan,^{†1,3*} Xingtao Xu,^{4*} Ahmed A. Farghali,⁵ Mohamed Hamdy Khedr,^{2,5}
Abdulmohsen Ali Alshehri,⁶ Yoshio Bando,^{1,7} Nanjundan Ashok Kumar⁸ and Yusuke Yamauchi^{8,9*}

- [1] International Center for Materials Nanoarchitectonics (MANA), National Institute for Materials Science (NIMS), 1-1 Namiki, Tsukuba, Ibaraki 305-0044, Japan
- [2] Chemistry Department, Faculty of Science, Beni-Suef University, Beni-Suef 62511, Egypt
- [3] Faculty of Science and Engineering, Waseda University, 3-4-1 Okubo, Shinjuku, Tokyo 169-8555, Japan
- [4] College of Hydrology and Water Resources, Hohai University, No. 1 Xikang Rd., Nanjing 210-098, China
- [5] Materials Science and Nanotechnology Department, Faculty of Postgraduate Studies for Advanced Sciences (PSAS), Beni-Suef University, Beni-Suef 62511, Egypt
- [6] Department of Chemistry, King Abdulaziz University, P.O. Box. 80203, Jeddah 21589, Saudi Arabia
- [7] Australian Institute for Innovative Materials (AIIM), University of Wollongong (UOW), North Wollongong, NSW 2500, Australia
- [8] School of Chemical Engineering and Australian Institute for Bioengineering and Nanotechnology (AIBN), The University of Queensland, Brisbane, QLD 4072, Australia
- [9] Department of Plant & Environmental New Resources, Kyung Hee University, 1732 Deogyong-daero, Giheunggu, Yongin-si, Gyeonggi-do 446-701, South Korea

† The authors contribute equally to this work.

E-mail: TAN.Haibo@nims.go.jp; xuxingtao1990@126.com; y.yamauchi@uq.edu.au

Abstract

Ordered mesoporous nitrogen-doped carbon (OMNC) materials are considered as the most promising material for supercapacitors. In this study, highly ordered two-dimensional (2D) hexagonal mesostructured polymer is synthesized through a facile assembly of triblock polymer micelles and phenol-melamine formaldehyde resin *via* organic-organic assembly process in aqueous solution. After calcination, the novel OMNC with 2D hexagonal mesostructures are obtained. By applying post-treatment of KOH activation, the surface area and the porosity of the OMNC are significantly improved, but the internal mesoporous structures are still maintained. The activated OMNC-800A displays specific capacitance as high as 475.75 F g^{-1} at 0.5 A g^{-1} and outstanding cycling stability (over 100% capacitance retention during 2,000 cyclic tests at 100 mV s^{-1}). These results confirm that the tubular mesochannels inside the OMNC are very beneficial to providing an accessible path for diffusion of electrolyte, thereby improving the specific capacitance of OMNC under a high current density.

Keywords: mesoporous carbon, nitrogen doping, hexagonal mesostructure, chemical activation, supercapacitor

1. Introduction

Mesoporous carbon materials show several exceptional properties including ultrahigh surface areas, large pore volumes, controllable mesoporous structures, *etc.*^{1,2} These materials are ideal candidates for a myriad of applications, particularly, electrochemical energy conversion and storage.³⁻⁵ To date, hard- and soft-templating approaches have been employed for the successful preparation of ordered mesoporous (OMC) carbon materials with controlled morphology, uniform pore structures and narrow pore size distribution. Hard-templating approach including mesoporous silicas have been utilized for synthesis of mesoporous carbon materials.⁶⁻⁸ However, the hard-templating approach is a multistep process (*i.e.*, preparation of ordered templates, replication of mesopores with appropriate carbon precursors, carbonization, and removal of template matrix). In this case, the rational design and control of templates are the key factors for producing high-quality mesoporous materials which is slightly complex, time and cost consuming, and unfavorable for mass production. In contrast, the soft-template method is a straightforward approach which is dependent on the self-assembly of the organic compounds and block copolymers into ordered mesostructured composites by oriented manner through a chemical interaction.⁹⁻¹³ Interestingly, the morphology, porosity and structure could be tuned by controlling the synthetic conditions, such as concentration of surfactant, pH, and carbonization temperature. The morphological controlling will endow the product with an excellent chemical activity, mechanical stability, good electrical conductivity, and high surface area, which have been considered as the essential requirements for electrode materials used in energy storage applications.^{14,15}

Supercapacitors as a backup power have received considerable attention in customer electronics, communication, and transportation systems benefited by its superior power density and long cycling durability.^{16,17} Research efforts are still directed toward increasing the power density and extending the long-term durability of electrodes to fulfill the requirements of high power delivery/uptake in portable electronics and other equipment with high power demands.^{18,19} Controlling pore size distribution is another crucial factor for carbon electrodes to boost high powder density by exposing accessible surface and providing diffusion path for electrolytes.²⁰⁻²³ Besides, it was also proved that not only the high surface area but also other parameters, such as nitrogen doping²⁴ and carbon particle size,²⁵ are crucial for improving the specific capacitance and the

rate performance of carbon electrodes in supercapacitors. Therefore, it is expected that the fabrication of ordered mesoporous nitrogen-doped carbon (OMNC) may integrate the advantages of OMC with nitrogen doping. We can expect the presence of tubular mesochannels is very beneficial to exposing accessible surface area and accelerating the diffusion of electrolytes. However, there are still challenges to synthesize OMNC with 2D hexagonal mesostructures due to complicated optimization of synthetic conditions.²⁶⁻³¹

In this study, highly ordered two-dimensional (2D) hexagonal mesostructured polymer is synthesized through a facile assembly of triblock polymer micelles and phenol-melamine formaldehyde resin *via* organic-organic assembly process in aqueous solution. The symmetric triblock polymer Pluronic P123 was used as mesopore-direct agent, phenol/formaldehyde and melamine/formaldehyde resin were used as carbon and nitrogen sources, respectively. After calcination, the as-made OMNC possessed uniformly-sized mesopores and plentiful tubular mesochannels. With further KOH activation at high temperatures, the morphology and ordered mesopores of OMNC were still maintained, and they also showed ultrahigh surface area (over 2,400 m² g⁻¹) mainly by creating abundant micropores. As a proof of concept, the electrochemical measurements demonstrate that the activated OMNC showed outstanding specific capacitance as high as 475.75 F g⁻¹ at 0.5 A g⁻¹ and remarkable long-term durability.

2. Experimental section

2.1. Chemicals. Pluronic P123 (PEG-PPG-PEG), Melamine, and 5.0 wt% Nafion perfluorinated resin solution were purchased from Sigma-Aldrich. Phenol, Formaldehyde (37 wt%), 0.1 M Sodium hydroxide, and 1 M H₂SO₄ were purchased from Nacalai Tesque, Inc. All the chemicals were analytical grade and used as received.

2.2. Preparation of ordered mesoporous nitrogen-doped carbon (OMNC). Firstly, the mesostructured polymer was prepared *via* organic-organic assembly process in aqueous solution with the assistance of triblock copolymer Pluronic P123. Phenol-melamine/formaldehyde resin (P-M/F) was added as carbon and nitrogen sources. Typically, 0.28 g of phenol and 0.19 g of melamine were dissolved in 1.5 mL of formaldehyde aqueous solution (37 wt%) under stirring at 60 °C, leading to a colorless transparent solution after 5 min. Then, 2.0 mL 0.1 M NaOH solution was added into the above clear solution and stirred at 70 °C for 30 min. Afterwards, 10.0 mL P123 aqueous solution (containing 0.325 g of P123) was added and the solution was stirred at 65 °C for 2 h. Subsequently, 25.0 mL of distilled water was added to the mixture and the diluted solution was further kept at 65 °C for another 10 h under mild stirring, resulting in a dark-red solution. After that, 10.0 mL of the obtained dark-red solution was transferred in a Teflon liner under vigorous stirring. The pH value was adjusted to *ca.* 9.3 by adding an appropriate volume of 0.1 M NaOH solution. The Teflon liners were transferred into autoclaves (100 mL) for hydrothermal reaction at 130 °C for 20 h with a ramping rate of 1 °C min⁻¹. The obtained precipitate was collected by centrifugation (14000 rpm for 5 min) and washed with water and ethanol three times. After drying at 60 °C, the mesostructured polymers were obtained. The synthetic conditions (*e.g.*, concentration of P123 and pH) for controlling the morphology of precursor were carefully investigated and the corresponding products were denoted as N/C-*x* (*x* = 1, 2, 3, 4, and 5). The detailed synthesis parameters were listed in **Table 1**. The as-made precursor was carbonized at controlled temperatures for 4 h under N₂ atmosphere. The ramping rate of the calcination process was 5 °C min⁻¹. The pre-carbonized ordered mesoporous nitrogen-doped carbons were assigned as OMNC-*T*, where *T* represents the calcination temperatures (700, 800, and 900 °C).

2.3. KOH activation of OMNC-*T*. Typically, the obtained 25.0 mg OMNC-*T* was mixed with 100.0 mg potassium hydroxide (KOH). Then, the mixture was dispersed in 5 mL of deionized water under sonication for

30 min. The slurry was dried at 100 °C overnight, following by thermal treatment at 800 °C for 2 h under flowing N₂ with a ramping rate of 5 °C min⁻¹. After cooling to the room temperature, the resultant powder was washed with deionized water to remove KOH completely. Finally, the activated OMNC-*T* was dried in an oven at 80 °C and labeled as OMNC-*TA*.

2.4. Characterization. The morphology of the samples was characterized by field emission scanning electron microscope (SEM, HITACHI SU-8230) operating at 5.0 kV. Transmission electron microscope (TEM, JEOL JEM-2100F) operated at 200 kV was employed to investigate the inner mesoporous structure. Small angle X-ray scattering (Rigaku NANO-Viewer) equipped with a camera length of 700 mm was used to evaluate the pore-to-pore distance with a Cu K α radiation (40 kV, 30 mA). Wide-angle X-ray diffraction (XRD) patterns were acquired with a Rigaku Rint 2000 X-ray diffractometer using monochromated Cu K α radiation (40 kV, 40 mA) at a scanning rate of 1° min⁻¹. Nitrogen adsorption-desorption isotherms were obtained using a BELSORP-mini (Bel Japan, Inc.) at 77 K. The specific surface area (SSA) was evaluated by the multipoint Brunauer-Emmett-Teller (BET) method at a relative pressure from 0.05 to 0.3 based on the adsorption data. The chemical state of nitrogen was investigated using X-ray photoelectron spectroscopy (PHI Quantera SXM) with Al K α radiation (20 kV, 5 mA). The shift of binding energy was calibrated using the C1 s level at 284.5 eV.

2.5. Electrochemical measurements. The as-prepared OMNC-*T* and OMNC-800A were ground before preparing inks. In a typical experiment, 2.0 mg of sample was dispersed in 400 μ l of 1:2 (v/v) isopropanol/water mixed solvent (containing 20 μ L of 5.0 wt% Nafion solution) under sonication for at least 30 min to form a homogenous ink. After that, 200 μ L of the suspension was dropped onto the flexible graphite paper (thickness: 1 mm) with an area of 1 \times 1 cm² and dried at 60 °C. The mass loading was 1.0 mg cm⁻² and the thickness of electrode film was measured to be around 15-25 μ m. In addition, we choose flexible graphite paper as the current collector because of its excellent electrical conductivity as well as its negligible capacitive performance (usually below 1 F g⁻¹), which would contribute little to the total capacitance of the prepared working electrode. All electrochemical measurements were carried out on a CHI 660E instrument. In a three-electrode system, the electrochemical performances of as-made OMNC-*T* and OMNC-800A electrodes were investigated by cyclic voltammetry (CV) and galvanostatic charge-discharge (GCD) in 1 M H₂SO₄, with a platinum wire as the

counter electrode and an Ag/AgCl electrode as the reference electrode. The specific capacitance for as-made electrodes was calculated from the GCD curves. The test of long-term stability for OMNC-800A was conducted by cycling between 0.0 and 0.8 V vs. Ag/AgCl in 1 M H₂SO₄ at a scan rate of 100 mV s⁻¹.

In general, the gravimetric specific capacitance (C_g , F g⁻¹) was calculated using the following equation:

$$C_g = \frac{I \times t}{m \times \Delta V} \quad (1)$$

where I is the discharge current (A), t is the discharge time (s), m is the mass of active material (g), and ΔV is the potential change during the discharge process (V).

3. Results and discussion

Figure 1 shows SEM images of as-prepared polymer particles with P123 concentrations at different pH values. As shown in **Figure 1c**, the optimized polymer particles show the morphology of hexagonal prism with size distribution of 200-400 nm. Thus, to gain deep understanding of morphology control, the role of P123 concentration and pH was investigated systematically (**Table 1**). The optimized mesostructured polymer (N/C-2) was obtained at pH value of 9.3 with P123 concentration of 32.5 mg mL^{-1} , while spherical particles (N/C-1, pH=8.5) and irregular nanoparticles (N/C-3, pH=10.0) were obtained (**Figure 1a-c**). This is more likely related to the polymerization rate of low molecular phenol-melamine/formaldehyde resin (P-MF), determined by the concentration of NaOH catalyst. **Figures 1d-e** display the morphology changes derived from altered concentration of P123 with the optimized pH value of 9.3. As can be clearly seen that the morphology of polymer particles was changed from spherical (N/C-4) to hexagonal prism (N/C-2) and finally to irregular cross-linked particles (N/C-5) with the increase of P123 concentration. As evidenced by small angle X-ray scattering (SAXS) analysis (**Figures S1**), the SAXS pattern of the optimized polymer particles (N/C-2) showed the obvious peak, while less ordered mesostructure of polymer particles was confirmed for non-optimized polymers (*i.e.*, N/C-1, -3, -4, and -5).

After calcination of N/C-2 at different temperatures, as shown in **Figures 2a-c**, **S2a-b**, and **S3a-b**, the SEM images display the maintained morphology and mesostructures regardless of the calcination temperature, indicating remarkable thermal stability of carbon framework of OMNC. After the removal of P123 micelles during carbonization, the TEM images reveal the ordered mesopores for OMNC-700, OMNC-800, and OMNC-900 with size of *ca.* 2.7, 3.6, and 3.0 nm (**Figures 2b-c**, **S2b**, and **S3b**), respectively. From TEM observation of individual particle (**Figure S4**), it was clearly seen that the tubular mesochannels are running in the same direction within one particle, which can act as diffusion pathways for the electrolytes. As seen in **Figures 2d-f**, **S2c-d**, and **S3c-d**, the original morphology and mesostructures were maintained even after KOH activation at high temperature. The retention of 2D hexagonal mesostructures was also confirmed by SAXS patterns (**Figures 3a** and **S5a**), further demonstrating the excellent structural stability of carbon walls between mesopores. Notably, it is ordinary to achieve the irregularly-shaped ordered mesoporous carbon (OMC) with

2D hexagonal $p6m$ symmetry,³¹⁻³³ while the hexagonal ordered mesoporous nitrogen-doped carbon (OMNC) particles have been rarely reported.

The SAXS patterns in **Figures 3a** and **S5a** show three resolved peaks which can be indexed as (10), (11) and (20) reflections. Compared with N/C-2 (**Figure 1b**), the (10) peaks are shifted to higher values because of the polycondensation of P-MF resin and the shrinkage of carbon frame work after calcination. As listed in **Table 2**, the d_{10} spacing reduces from 12.17 nm (N/C-2) to 8.85 nm (OMNC-700), 8.44 nm (OMNC-800), and 8.39 nm (OMNC-900) with increasing calcination temperature from 700 to 900 °C. After activation with KOH, as seen in **Figure 3a** and **Figure S7a**, SAXS patterns show reduced intensity of activated samples, especially for OMNC-900, indicating the deterioration of ordered mesoporous structure due to the etching of carbon walls and the newly generation of micropores.^{32,33}

The wide-angle X-ray diffraction (XRD) patterns for all samples show two characteristic graphitic peaks located at around 23° and 44° which can be assigned to (002) and (101) planes (**Figures 3b** and **S5b**), respectively. After KOH activation, the peak of (002) plane disappeared except for OMNC-900A because OMNC-900 pre-carbonized at higher temperature was more stable than OMNC-700 and OMNC-800 during activation. This variation should be ascribed to the etching reaction between carbon framework and KOH which consumed the carbon skeleton and created more pores.^{34,35}

High resolution X-ray photoelectron spectroscopy (XPS) was conducted for the representative OMNC-800 and activated OMNC-800A (**Figure 3c**) to characterize the chemical state of nitrogen. The N 1s XPS spectra of OMNC-800 and OMNC-800A were deconvoluted into four peaks at 398.2 eV (pyridinic N), 399.5 eV (pyrrolic N), 400.9 eV (graphitic N), and 403.2 eV (oxidized N).^{36,37} The N content of 6.5 at% (OMNC-800) was decreased to 0.9 at% (OMNC-800A) after KOH activation due to partial replacement of nitrogen by oxygen through the activation reaction.³⁸ The relative content of all N species in OMNC-800 and OMNC-800A was estimated by XPS analysis and summarized in **Figure S6**. After KOH activation, the percentage of pyridinic N was dropped from 29.43 at% for OMNC-800 to 4.65 at% for OMNC-800A. In contrast, the percentage of graphitic-N increased from 49.60 at% for OMNC-800 to 53.96 at% for OMNC-800A. These findings are consistent with the fact that graphitic N is more stable than pyridinic N.³⁹ In general, pyridinic N

and graphitic N in carbons were regarded as electroactive sites, which would benefit the enhancement of electrical conductivity as well as capacitances.^{40,41}

Based on the analysis of N₂ adsorption-desorption isotherms (**Figures 3d** and **S5c**), the increase of the calcination temperature from 700 to 800 and 900 °C led to the gradual increase in specific surface area (SSA) from 696 to 840 and 893 m² g⁻¹, respectively. The KOH activation process caused a significant enhancement of SSA for all activated samples, as shown in **Table 2**. It can be clearly observed that the much higher N₂ uptake at a low relative pressure ($P/P_0 < 0.1$) for activated products (OMNC-*T*), which indicates the formation of tremendous micropores after activation. The SSA of OMNC-800A is obviously higher than other activated samples, reaching up to 2450 m² g⁻¹. That was attributed to the highest pore volume of OMNC-800 which was beneficial to the deep impregnation of molten KOH. In addition, as mentioned above, OMNC-900 calcinated under high temperature was more difficult to be activated deeply by KOH.

Considering the unique structural advantages of OMNC-*T*, including well-dispersed particles, uniformly-sized mesopores, tubular mesochannels, and high surface area, it is expected to be a promising electrode material for practical supercapacitors. To show the superiority of OMNC-800A, the electrochemical performances of the OMNC-*T* and OMNC-800A were investigated in a three-electrode system using 1 M H₂SO₄ as electrolyte. Cyclic voltammetry (CV) curves shown in **Figure 4a** indicate that all samples display rectangle-like curves, revealing the typical electrical double layer capacitive properties of all samples. Remarkably, OMNC-800 exhibited a higher CV area than those of OMNC-700 and OMNC-900, suggesting that OMNC-800 has a better capacitive property compared to OMNC-700 and OMNC-900. In addition, after activation by KOH, the obtained OMNC-800A showed an improved capacitive performance compared to pristine OMNC-800. The specific capacitances at 0.5 A g⁻¹ (denoted as $C_{0.5}$) were calculated by galvanostatic charge-discharge (GCD) measurements (**Figure 4b**) for all samples (OMNC-*T* and OMNC-800A). The corresponding values of $C_{0.5}$ are 196.81 (OMNC-700), 332.12 (OMNC-800), 314.56 (OMNC-900), and 475.75 F g⁻¹ (OMNC-800A). Obviously, OMNC-800A displayed the highest specific capacitance of 475.75 F g⁻¹. To the best of our knowledge, this value is also higher than those for all the reported N-doped carbon values measured in aqueous electrolyte utilizing a three-electrode system (**Table S1**). In addition, the GCD plots

shown in **Figure 4b** are generally symmetric, which is indicative of high capacitive reversibility and very low internal resistance of all samples.

Figure 4c shows the specific capacitances of the OMNC-*T* and OMNC-800A calculated based on the discharge curves at various current densities from 0.5 to 10 A g⁻¹. As expected, the capacitance values of OMNC-800A far surpass those of non-activated samples at any current density. In addition, even at a relatively high current density of 10 A g⁻¹, the capacitance value of OMNC-800A can still achieve high value of 325 F g⁻¹ (**Figure S7**), displaying remarkable rate capacitance retention (68%). Such excellent capacitance retention is an indication for quick charge propagation capability and easy ion transport within the OMNC-800A electrode material. To further demonstrate the superiority of OMNC-800A, the long-term stability of OMNC-800A was investigated by CV measurement at 100 mV s⁻¹ (**Figures 4d** and **S8**). Remarkably, the capacitance for the first 2000 cycles gradually increased until capacitance retention reached 113%, possibly due to the activation process of the OMNC-800A electrode by improved wetting of the electrolyte deep inside mesochannels of the electrode material. After 10000 cycles, it retained 90% of its initial capacitance value, indicating a good stability of OMNC-800A electrode.

The above results indicate that OMNC-800A is a promising carbon material for supercapacitors. The superior capacitive performance of OMNC-800A can be ascribed to the following reasons: (i) OMNC-800A exhibited an ultrahigh specific surface area and large pore volume (2450 m² g⁻¹ and 1.34 cm³ g⁻¹). As well known, high specific surface and large pore volume of porous carbons usually result in high electrochemical double layer capacitance.^{42,43} (ii) OMNC-800A exhibited a novel hierarchically porous structure with plentiful mesochannels, not only guaranteeing that OMNC-800A electrode can be wetted quickly by the electrolyte, but also help to accelerate the ion transport.

4. Conclusion

In this study, we demonstrated the preparation of mesostructured polymer particles by soft-templating approach using P123 triblock copolymer. Phenol-melamine/formaldehyde resin was used as the carbon precursor and nitrogen source. After carbonization, OMNC with 2D hexagonal mesostructures were obtained. The further activated OMNC by KOH maintained the original 2D hexagonal mesostructures. Activated OMNC-800A featured with high specific surface area ($2,450 \text{ m}^2 \text{ g}^{-1}$) and revealed an outstanding gravimetric specific capacitance of 475.75 F g^{-1} at a current density of 0.5 A g^{-1} and excellent stability with high capacitance retention in a three-electrode system. Moreover, the synthetic approach developed in this study is simplicity, environmental friendliness, and reliability, which are beneficial to quantity production for practical application in supercapacitors.

Acknowledgement

This work was supported by an Australian Research Council (ARC) Future Fellow (grant no. FT150100479), JSPS KAKENHI (grant nos. 17H05393 and 17K19044), and the research fund by the Suzuken Memorial Foundation. This work was also supported by the Deanship of Scientific Research (DSR), King Abdulaziz University, Jeddah. A.E.A appreciates the financial support by joint supervision scholarship from Cultural affairs and missions sector, Egyptian ministry of higher education (MOHE).

References

- 1 C. Liang, Z. Li and S. Dai, *Angew. Chem. Int. Ed.*, 2008, **47**, 3696-3717.
- 2 T. Y. Ma, L. Liu and Z.-Y. Yuan, *Chem. Soc. Rev.*, 2013, **42**, 3977-4003.
- 3 F. Su, J. Zeng, X. Bao, Y. Yu, J. Y. Lee and X. S. Zhao, *Chem. Mater.*, 2005, **17**, 3960-3967.
- 4 G. Bingkun, W. Xiqing, F. P. F., C. Miaofang, M. S. M., S. Xiao-Guang and D. Sheng, *Adv. Mater.*, 2011, **23**, 4661-4666.
- 5 G. Shen, X. Sun, H. Zhang, Y. Liu, J. Zhang, A. Meka, L. Zhou and C. Yu, *J. Mater. Chem. A*, 2015, **3**, 24041-24048.
- 6 S. Jun, S. H. Joo, R. Ryoo, M. Kruk, M. Jaroniec, Z. Liu, T. Ohsuna and O. Terasaki, *J. Am. Chem. Soc.*, 2000, **122**, 10712-10713.
- 7 S. Leyva-García, D. Lozano-Castelló, E. Morallón and D. Cazorla-Amorós, *J. Mater. Chem. A*, 2016, **4**, 4570-4579.
- 8 J. Lee, S. Yoon, T. Hyeon, S. M. Oh and K. B. Kim, *Chem. Commun.*, 1999, **0**, 2177-2178.
- 9 D. Liu, L. J. Xia, D. Qu, J. H. Lei, Y. Li and B. L. Su, *J. Mater. Chem. A*, 2013, **1**, 15447-15458.
- 10 W. C. Chu, B. P. Bastakoti, Y. V. Kaneti, J. G. Li, H. R. Alamri, Z. A. Allothman, Y. Yamauchi and S. W. Kuo, *Chem. Eur. J.*, 2017, **23**, 13734-13741.
- 11 J. Tang, J. Liu, C. Li, Y. Li, M. O. Tade, S. Dai, Y. Yamauchi, *Angew. Chem. Int. Ed.*, 2015, **54**, 588-593.
- 12 J. Tang, J. Liu, R. R. Salunkhe, T. Wang and Y. Yamauchi, *Chem. Commun.*, 2016, **52**, 505-508.
- 13 H. Tan, Y. Li, X. Jiang, J. Tang, Z. Wang, H. Qian, P. Mei, V. Malgras, Y. Bando and Y. Yamauchi, *Nano Energy*, 2017, **36**, 286-294.
- 14 A. Eftekhari and Z. Fan, *Mater. Chem. Front.*, 2017, **1**, 1001-1027.
- 15 E. Lim, C. Jo and J. Lee, *Nanoscale*, 2016, **8**, 7827-7833.
- 16 X. Xu, J. Tang, H. Qian, S. Hou, Y. Bando, M. S. A. Hossain, L. Pan and Y. Yamauchi, *ACS Appl. Mater. Interfaces*, 2017, **9**, 38737-38744.
- 17 R. R. Salunkhe, Y. H. Lee, K. H. Chang, J. M. Li, P. Simon, J. Tang, N. L. Torad, C. C. Hu and Y. Yamauchi, *Chem. Euro. J.*, 2014, **20**, 13838-13852.
- 18 X. Yu, J. Wang, Z.-H. Huang, W. Shen and F. Kang, *Electrochem. Commun.*, 2013, **36**, 66-70.
- 19 M. Li, J. Ding and J. Xue, *J. Mater. Chem. A*, 2013, **1**, 7469-7476.
- 20 J. Tang, J. Wang, L. K. Shrestha, M. S. A. Hossain, Z. A. Allothman, Y. Yamauchi and K. Ariga, *ACS Appl. Mater. Interfaces*, 2017, **9**, 18986-18993.
- 21 J. Huang, B. G. Sumpter and V. Meunier, *Chem. Eur. J.*, 2008, **14**, 6614-6626.
- 22 L. Borchardt, M. Oschatz and S. Kaskel, *Mater. Horiz.*, 2014, **1**, 157-168.
- 23 L. Zhang, X. Yang, F. Zhang, G. Long, T. Zhang, K. Leng, Y. Zhang, Y. Huang, Y. Ma, M. Zhang and Y. Chen, *J. Am. Chem. Soc.*, 2013, **135**, 5921-5929.

- 24 T. Lin, I.-W. Chen, F. Liu, C. Yang, H. Bi, F. Xu and F. Huang, *Science*, 2015, **350**, 1508-1513.
- 25 A. J. R. Rennie, V. L. Martins, R. M. Smith and P. J. Hall, *Sci. Rep.*, 2016, **6**, 22062.
- 26 F. Zhang, D. Gu, T. Yu, F. Zhang, S. Xie, L. Zhang, Y. Deng, Y. Wan, B. Tu and D. Zhao, *J. Am. Chem. Soc.*, 2007, **129**, 7746-7747.
- 27 D. Gu, H. Bongard, Y. Meng, K. Miyasaka, O. Terasaki, F. Zhang, Y. Deng, Z. Wu, D. Feng, Y. Fang, B. Tu, F. Schüth and D. Zhao, *Chem. Mater.*, 2010, **22**, 4828-4833.
- 28 J. Yu, M. Guo, F. Muhammad, A. Wang, G. Yu, H. Ma and G. Zhu, *Microporous Mesoporous Mater.*, 2014, **190**, 117-127.
- 29 D. Liu, C. Zeng, D. Qu, H. Tang, Y. Li, B. L. Su and D. Qu, *J. Power Sources*, 2016, **321**, 143-154.
- 30 A. Chen, Y. Yu, Y. Zhang, W. Zang, Y. Yu, Y. Zhang, S. Shen and J. Zhang, *Carbon*, 2014, **80**, 19-27.
- 31 J. Zhu, J. Yang, R. Miao, Z. Yao, X. Zhuang and X. Feng, *J. Mater. Chem. A*, 2016, **4**, 2286-2292.
- 32 Y. Lv, F. Zhang, Y. Dou, Y. Zhai, J. Wang, H. Liu, Y. Xia, B. Tu and D. Zhao, *J. Mater. Chem.*, 2012, **22**, 93-99.
- 33 W. Teng, Z. Wu, J. Fan, H. Chen, D. Feng, Y. Lv, J. Wang, A. M. Asiri and D. Zhao, *Energy Environ. Sci.*, 2013, **6**, 2765-2776.
- 34 R. Heimböckel, S. Kraas, F. Hoffmann and M. Fröba, *Appl. Surf. Sci.*, 2018, **427**, 1055-1064.
- 35 F. Sun, J. Gao, X. Liu, X. Pi, Y. Yang and S. Wu, *Appl. Surf. Sci.*, 2016, **387**, 857-863.
- 36 I. Kusunoki, M. Sakai, Y. Igari, S. Ishidzuka, T. Takami, T. Takaoka, M. Nishitani-Gamo and T. Ando, *Surf. Sci.*, 2001, **492**, 315-328.
- 37 E. Raymundo-Piñero, D. Cazorla-Amorós, A. Linares-Solano, J. Find, U. Wild and R. Schlögl, *Carbon*, 2002, **40**, 597-608.
- 38 M. Wahid, G. Parte, D. Phase and S. Ogale, *J. Mater. Chem. A*, 2015, **3**, 1208-1215.
- 39 Y. Chen, Q. Liu and J. Wang, *Nano Adv.*, 2016, **1**, 79-89.
- 40 R. Czerw, M. Terrones, J. C. Charlier, X. Blase, B. Foley, R. Kamalakaran, N. Grobert, H. Terrones, D. Tekleab, P. M. Ajayan, W. Blau, M. Rühle and D. L. Carroll, *Nano Lett.*, 2001, **1**, 457-460.
- 41 Y. Deng, Y. Xie, K. Zou and X. Ji, *J. Mater. Chem. A*, 2016, **4**, 1144-1173.
- 42 J. Chmiola, G. Yushin, Y. Gogotsi, C. Portet, P. Simon and P. L. Taberna, *Science*, 2006, **313**, 1760-1763.
- 43 L. L. Zhang and X. S. Zhao, *Chem. Soc. Rev.*, 2009, **38**, 2520-2531.

Table 1 Different preparation condition with changing P123 concentrations or pH values.

Samples	Concentration of P123 (mg mL ⁻¹)	pH values
N/C-1	32.5	8.5
N/C-2	32.5	9.3
N/C-3	32.5	10.0
N/C-4	10.0	9.3
N/C-5	100.0	9.3

Table 2. Physicochemical properties of OMNC-*T* and OMNC-*TA* (*T* = 700, 800, 900).

Sample	d_{10} (nm)	Specific surface area (m ² g ⁻¹)	Pore volume (cm ³ g ⁻¹)
N/C-2	12.17	–	–
OMNC-700	8.85	696	0.37
OMNC-800	8.44	840	0.49
OMNC-900	8.39	893	0.45
OMNC-700A	8.57	1790	0.89
OMNC-800A	8.41	2450	1.34
OMNC-900A	8.14	1630	0.93

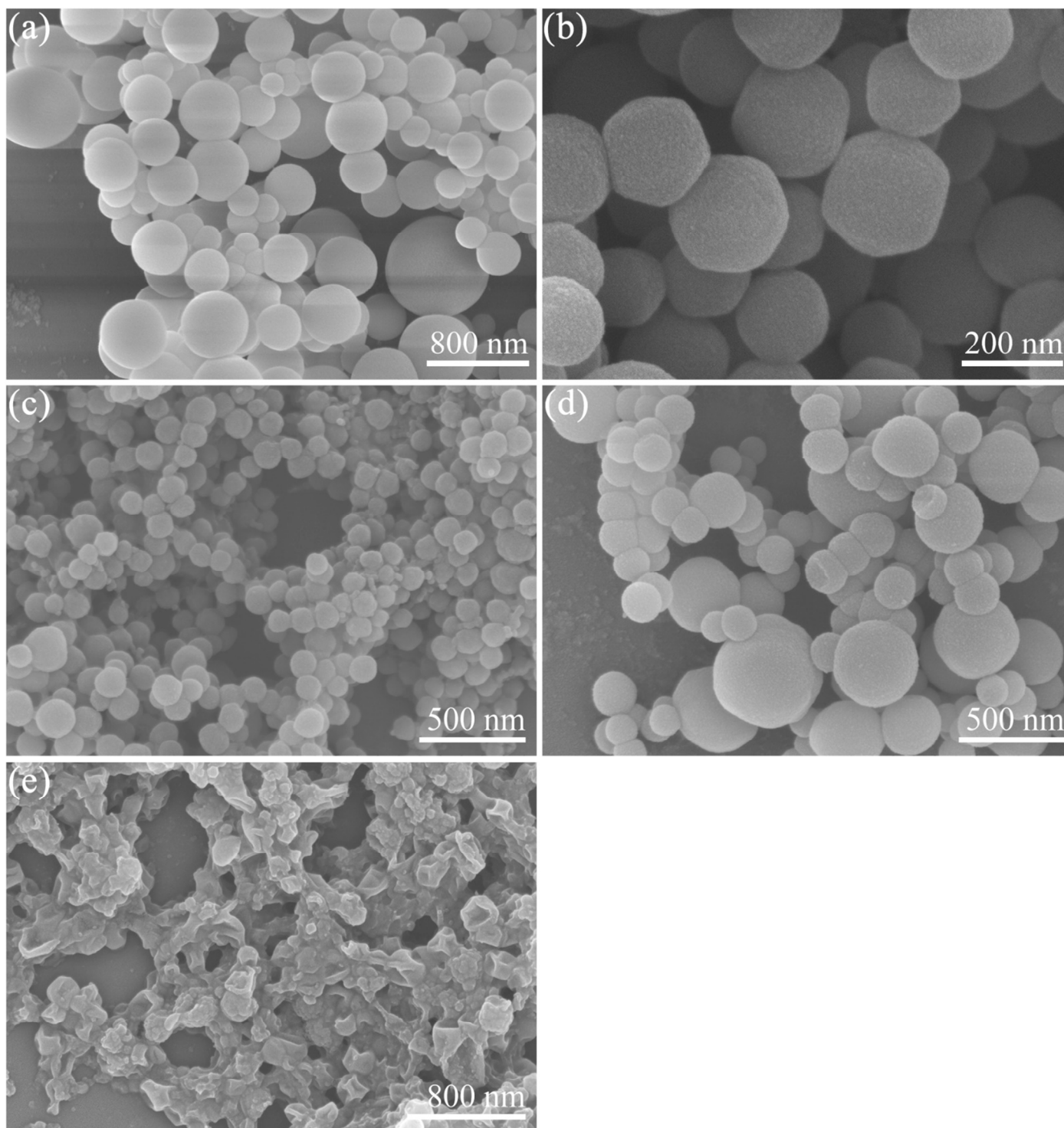


Figure 1 (a-c) SEM images of as prepared polymer particles with P123 concentration of 32.5 mg mL^{-1} at different pH value [(a) N/C-1 (pH=8.5), (b) N/C-2 (pH=9.3) and (c) N/C-3 (pH=10.0)]. (c, d) SEM images of as prepared polymer particles using different concentration of P123 at pH value of 9.3 [(c) N/C-4 (10.0 mg mL^{-1}) and (d) N/C-5 (100.0 mg mL^{-1})].

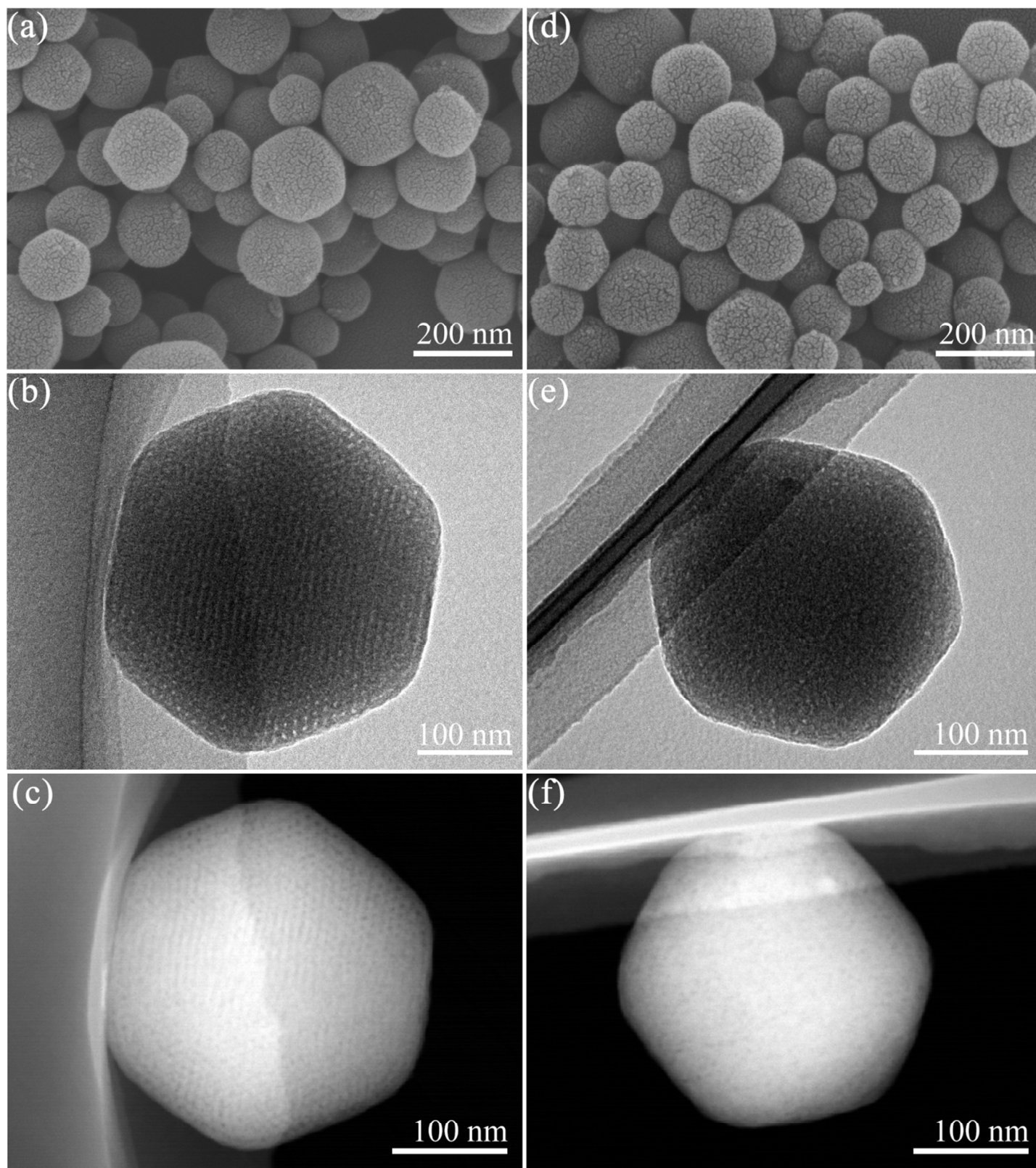


Figure 2 SEM, TEM, and HAADF-STEM images for representative samples: (a-c) OMNC-800 carbonized at 800 °C; (d-f) corresponding activated product OMNC-800A.

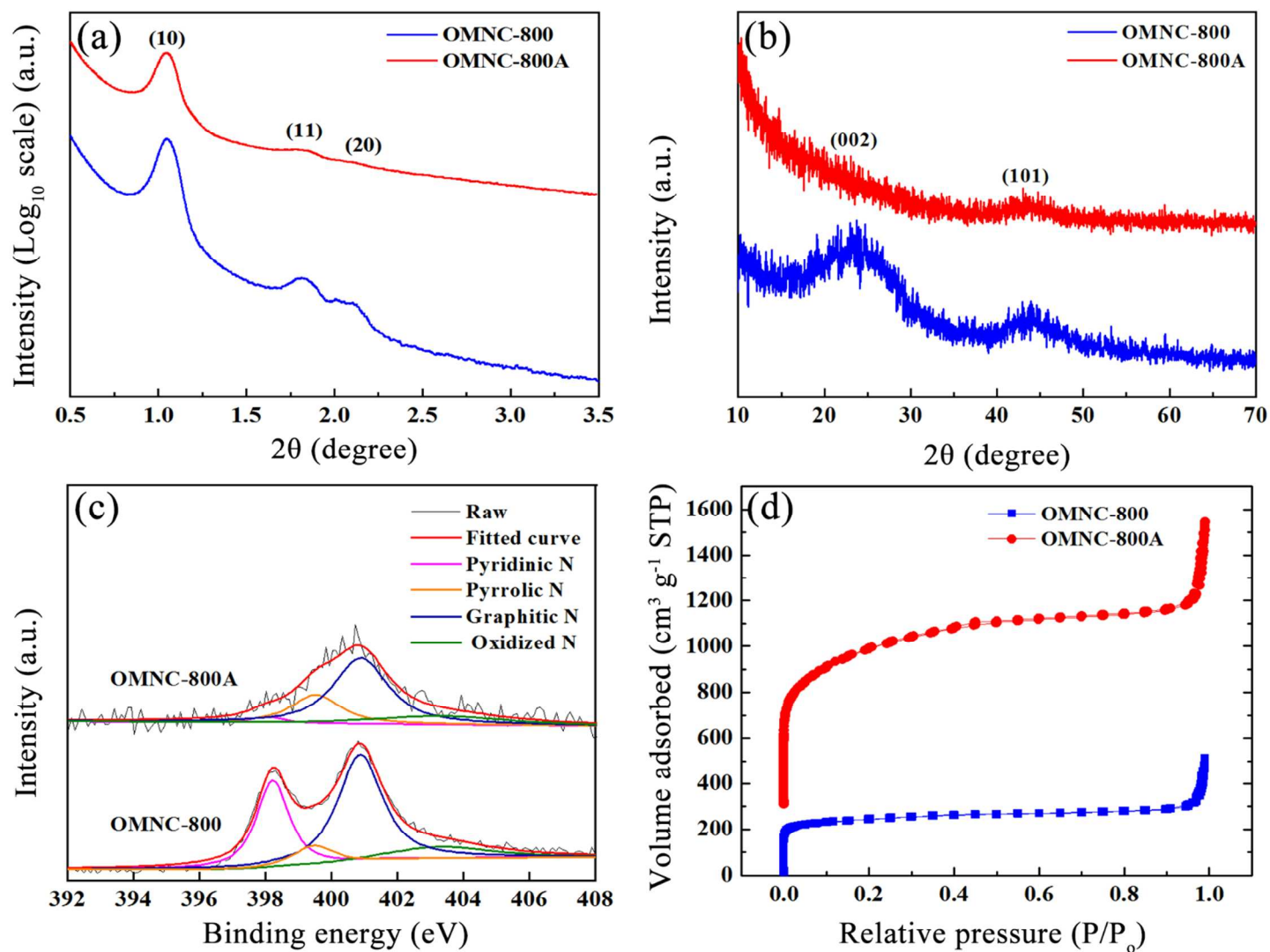


Figure 3 (a) SAXS patterns, (b) XRD patterns, (c) High-resolution N 1s XPS spectra, and (d) N₂ adsorption-desorption isotherms of OMNC-800 and OMNC-800A.

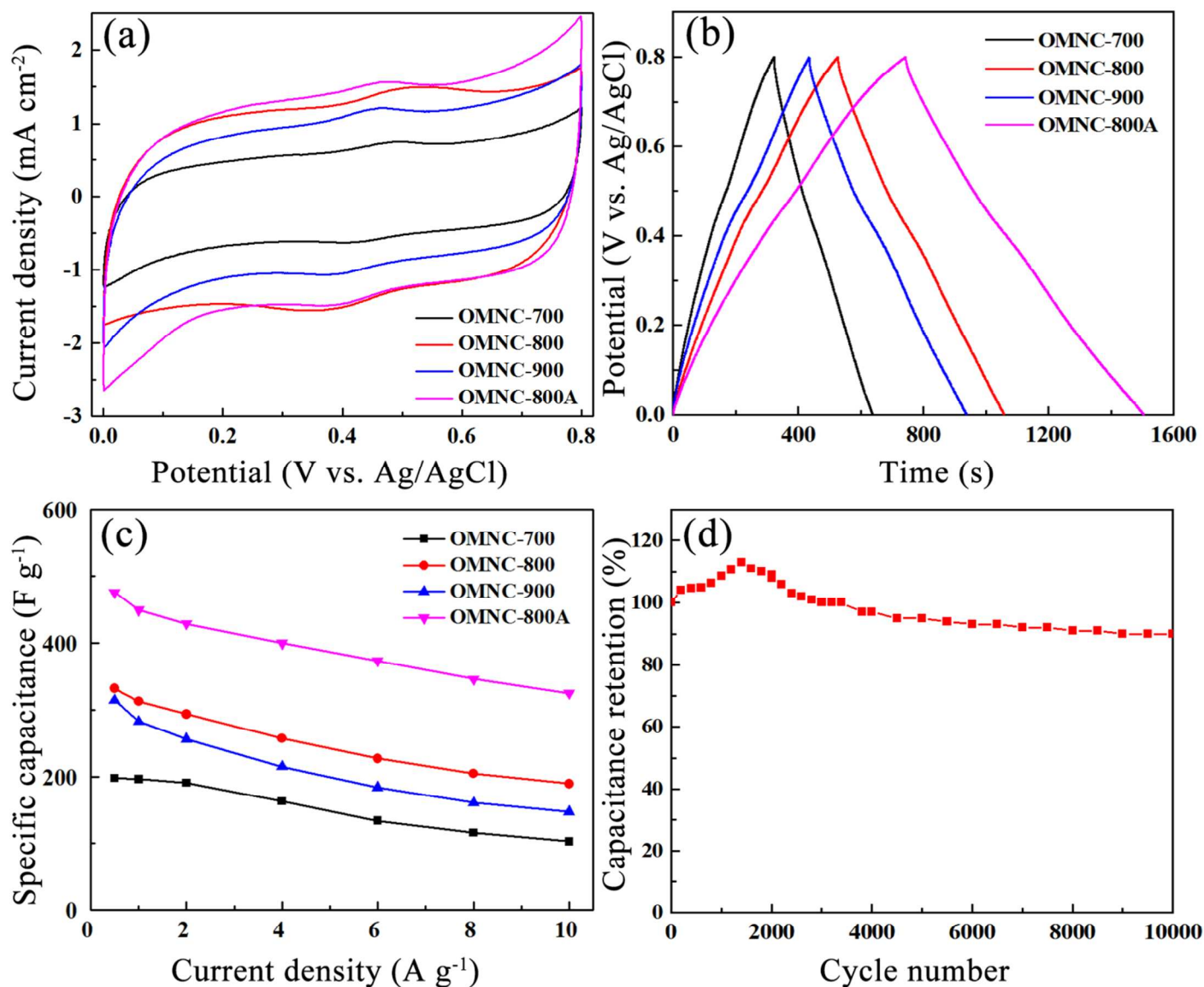


Figure 4 (a) CV curves at 5 mV s⁻¹ scan rate, (b) Galvanostatic charge-discharge curves at a current density of 0.5 A g⁻¹, and (c) Specific capacitances at different current densities for OMNC-*T* (*T* = 700, 800, 900) and OMNC-800A; (d) Cycling performance of OMNC-800A at 100 mV s⁻¹.

The as-obtained ordered mesoporous nitrogen-doped carbon hexagonal prism *via* facile soft-templated approach exhibits outstanding rate performance in supercapacitors.

